




## LEA—A NOVEL LOW ENERGY ACCELERATOR FOR <sup>14</sup>C DATING

Urs Ramsperger<sup>1\*</sup>  • Daniele De Maria<sup>1</sup> • Philip Gautschi<sup>1</sup> • Sascha Maxeiner<sup>2</sup> • Arnold Milenko Müller<sup>1</sup> • Hans-Arno Synal<sup>1</sup>  • Lukas Wacker<sup>1</sup> 

<sup>1</sup>ETH Zürich, Laboratory of Ion Beam Physics, Zurich, Switzerland

<sup>2</sup>Ionplus AG, Dietikon, Switzerland

**ABSTRACT.** A newly developed compact AMS, LEA (Low Energy Accelerator), is tested and compared with a state-of-the-art AMS system MICADAS (Mini Carbon Dating System), which has a precision performance of better than 1‰ for modern <sup>14</sup>C. The main difference between these two systems is the acceleration voltage, which has been reduced from 200 kV with the MICADAS system to 50 kV with the LEA system. In order to execute the final performance tests, exactly same samples (2 sets consisting of 7 standards, 4 blanks, 26 wood samples) are measured on both systems successively. The results show that the LEA system is fully operational, and the performance is entirely comparable with that of the MICADAS system.

**KEYWORDS:** accelerator mass spectrometry, radiocarbon AMS dating, tabletop AMS spectrometer, vacuum insulated high voltage device.

### INTRODUCTION

The great success with MICADAS (Mini Carbon Dating System, first prototype commissioned in 2004) in the AMS technology (Synal et al. 2007) triggered further development towards a tabletop AMS system. Changing the stripper gas from Ar to He has opened the possibility of lowering the accelerator voltage, as the yield of carbon isotopes stripping from the 1- state to the 1+ state is higher at lower energies (Schulze-König et al. 2011; Maxeiner et al. 2015a). Based on the MICADAS system, the acceleration voltage at the gas stripper unit, where charge exchange of the negative ions takes place and interfering isobar molecules are dissociated, is then reduced from 200 kV for MICADAS to 50 kV for the LEA (Low Energy Accelerator) system. By using He stripper gas at a local areal density of  $\approx 0.5 \mu\text{g}/\text{cm}^2$  molecular interferences can be destroyed at a particle energy of less than 100 keV (Schulze-König et al. 2011) without excessive beam losses that would impede reproducible measurements conditions. Detailed optimization of the acceleration stage hosting the stripper gas volume are necessary to balance molecule dissociation power and optical beam losses to enable measurement conditions suitable for routine high-performance radiocarbon dating measurements (Maxeiner et al. 2015b, 2019; Suter et al. 2022).

### SYSTEM DESCRIPTION

#### Design of the LEA AMS System

Figure 1 shows the schematic layout of the new LEA system. Basic elements such as the ion source, injection magnet, and the fast beam bouncing system are copied from the MICADAS design, while the mass spectrometer following the acceleration stage has been modified according to the reduced ion energy. As a consequence, the beam curve radius of the high energy magnet is reduced from 350 mm (MICADAS) to 250 mm (LEA) and the curve radius for the electrostatic deflector is reduced from 380 mm (MICADAS) to 250 mm (LEA)

\*Corresponding author. Email: [ramsperger@phys.ethz.ch](mailto:ramsperger@phys.ethz.ch)

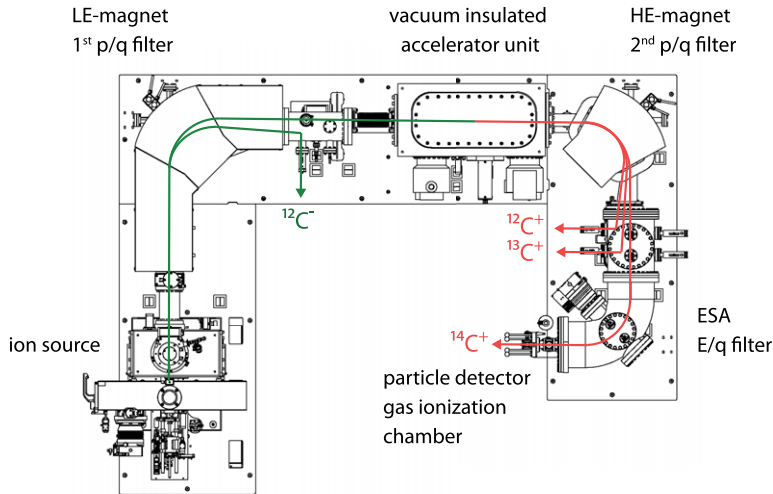


Figure 1 Schematic representation of the LEA AMS system operating at ETH Zurich. This compact AMS instrument has an overall footprint of just 3 m x 2 m. The beam injector (LE-side) reproduces the one of the MICADAS system. The size of the HE-side has been reduced due to the new design of the accelerator unit and the lower energy of the ions after the tandem acceleration stage (terminal voltage around 50 kV).

(De Maria 2021). This leads to a reduction of the overall footprint of the system to just  $2.0 \times 3.0 \text{ m}^2$ , which is  $1.5 \text{ m}^2$  less than the footprint of MICADAS.

### Accelerator Unit of LEA

Detailed view of the HE (High Energy) end of the LEA AMS system is shown in Figure 2. The geometry of the stripper tube defines the phase space volume that matches the geometric acceptance of the following HE spectrometer. The areal density of the stripper medium (He at  $\approx 0.5 \mu\text{g}/\text{cm}^2$ ) enables the reduction of the molecular component of the injected mass 14 ion beam below the detection limit of the instrument. However, molecular break up products such as  $^{12}\text{C}$  and  $^{13}\text{C}$  ions will emerge partly from the stripper tube in charge state  $2^+$ . These ions will gain more energy during their passage through the HE acceleration gap than the  $1^+$  ions.

If a charge exchange process  $2^+ \rightarrow 1^+$  of those ions happens at the appropriate distance in the acceleration field (e.g., by collisional process with residual gas atoms/molecules), they will reach exactly the same momentum/charge ( $p/q$ ) ratio as the  $^{14}\text{C}$  ion to be identified. Consequently, the filtering power of the HE magnet will be ineffective, and these parasitic ions will follow the  $^{14}\text{C}^+$  trajectories. Of course, they will have a different energy, but another collisional process further down the ion paths will create a certain probability that these ions will have a chance to reach the final detection system, mimic a false  $^{14}\text{C}$  ion, and create an elevated background. Such processes will happen in any AMS system exploiting a dual use of the acceleration voltage via the tandem principle. At the LEA system they might be enhanced due to the very low ion energy. To reduce this effect, the design of the LEA acceleration stage separates the exit of the conductance limiting aperture of the stripper housing from the acceleration gap. This reduces the density of the outflowing stripper gas in the critical region where the unwanted collisions can happen. Assuming a pressure distribution based on an error

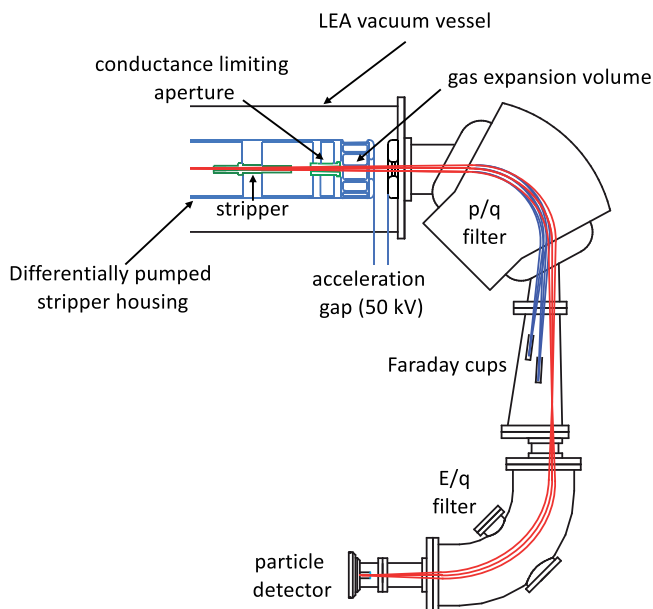


Figure 2 Schematic view of the high energy end of the LEA AMS system. The stripper housing is differentially pumped and the conductance limiting aperture is separated from the acceleration section. The following magnetic ( $p/q$ ) and the electrostatic ( $E/q$ ) filtering elements are combined to enable an achromatic image of the ions emerging from the stripper tube to the final ion detector. Red: ion trajectories of  $^{14}\text{C}$  ions, blue trajectories of  $^{12}\text{C}$  and  $^{13}\text{C}$  ions, as they are sequentially injected into the acceleration stage by the fast beam bouncing system.

function at the exit of the conductance limiting aperture of the stripper housing, using the pressure inside the stripper housing and the base vacuum within the acceleration vessel as end members, the probability of parasitic charge exchange processes can be calculated. Based on this calculation, a reduction of background events by at least one order of magnitude can be expected. Combined with the achromatic combination of  $p/q$  (magnetic), and  $E/q$  (electrostatic) filtering elements enables  $^{14}\text{C}$  detection limits of better than 50,000 yr BP corresponding to  $^{14}\text{C}/^{12}\text{C}$  ratio of less than  $2 \times 10^{-15}$  for processed blank materials.

### **$^{14}\text{C}$ Detector**

A Bragg-type gas ionization detector run with isobutane 3.5 is used to detect the  $^{14}\text{C}$  ions. Since the energy of the  $^{14}\text{C}$  ions is significantly lower than in the MICADAS system (less than 150 keV), the detector (Müller et al. 2015) is operated in the proportional counting region instead of the ion chamber region. Several test measurements taken with the LEA system showed that values of 450 V for the applied voltage and a gas pressure of 9.5 mbar provide the most accurate results in separating the background from the real  $^{14}\text{C}$  events. Since the  $^{14}\text{C}$  isotope energy is only 140 keV, the detector signal is amplified by a factor of approximately 3, resulting in a signal level of 3 V. By comparison, the MICADAS uses 300 V detector voltage at an isobutane

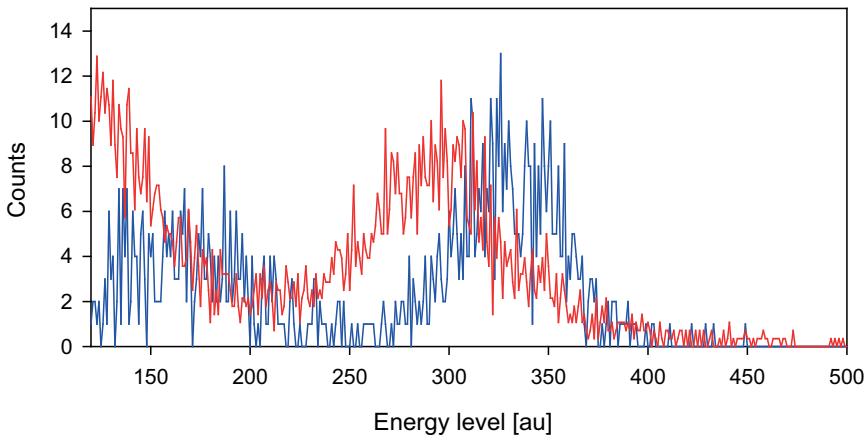


Figure 3 Two energy spectra of a PhA blank sample taken with an isobutane gas detector through 30 nm (blue lines) and 50 nm (red lines) Silicon Nitride membrane windows respectively. The horizontal axis refers to the energy level of the detected particles given in arbitrary units (au). Each spectrum is measured with the same blank sample for 30 min at a HE  $^{12}\text{C}$  current of  $>10\ \mu\text{A}$ . The gap between the background peak and the  $^{14}\text{C}$  peak is clearly visible in the measurement taken with the 30 nm window, while the two peaks overlap in the spectrum with the 50 nm window.

gas pressure of 20 mbar. With the same settings of the amplifier electronics and total  $^{14}\text{C}$  isotope energy of 420 keV and an amplification factor of 1, the signal level is also equal to 3 V.

The thickness of the entrance window separating the vacuum and the isobutane gas of the detector also plays an important role in ensuring a clean division between background noise and the  $^{14}\text{C}$  events, as seen in Figure 3. Two different Silicon Nitride membrane detector windows were tested with nominal thicknesses of  $d_1 = 30\ \text{nm}$  and  $d_2 = 50\ \text{nm}$ , respectively. Test measurements were conducted using graphitized phthalic acid (PhA) blank samples as target materials. They are presumably free of  $^{14}\text{C}$  due to their petrochemical origin but usually contain a  $^{14}\text{C}$  contamination record from the preparation process which is typically visible at a low  $10^{-15}$  ratio with respect to  $^{12}\text{C}$ . Therefore, the obtained spectra show a distinct  $^{14}\text{C}$  peak and background events which predominantly dissipate lower energy signals in the active detector volume. There is no evidence that these background events are related to the detector itself, but are due to scattered particles. The background events and the  $^{14}\text{C}$  events in the energy spectrum of the 50 nm window, indicated as a red line in Figure 3, overlap and cannot be properly separated. Conversely, due to the lower stopping energy and energy straggling (Sun et al. 2007; Suter et al. 2007) in the thinner 30 nm membrane window, the energy spectrum recorded, marked with a blue line in Figure 3, shows two well-separated peaks that clearly distinguish the  $^{14}\text{C}$  events from other background events.

## MEASUREMENTS AND PERFORMANCE TEST

### Beam Optimization

In order to achieve reliable and stable results, each isotope beam has to be adjusted with the fast-bouncing system in such a way that beam scans performed with the low energy (LE) magnet as well as with the high energy (HE) magnet are depicted as shown in Figure 4. The

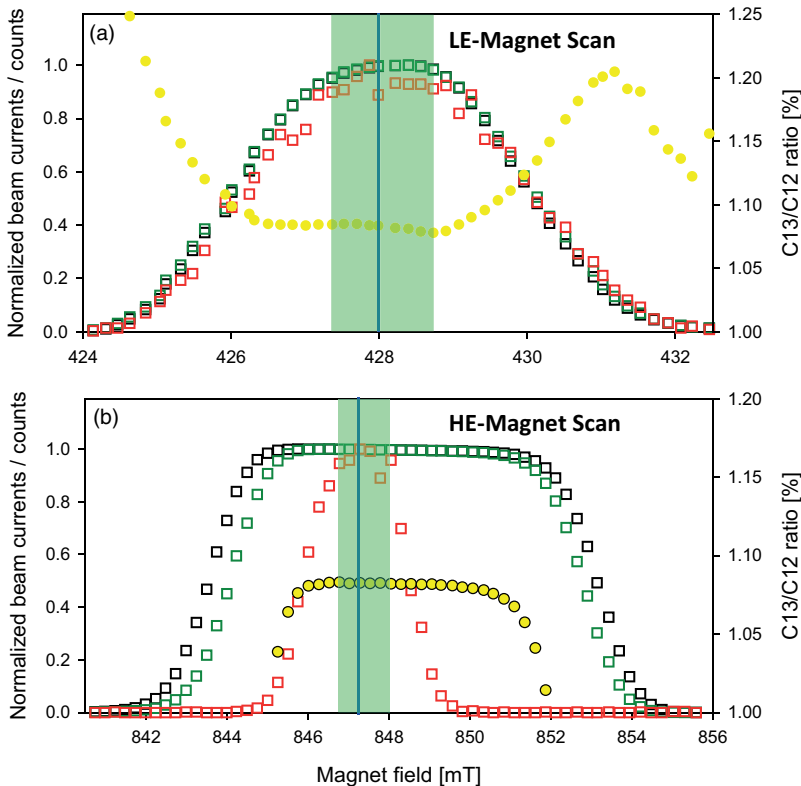


Figure 4 Low energy magnet (a) and high energy magnet (b) beam scans taken after optimizing the different isotopic beams. Black squares indicate normalized  $^{12}\text{C}$  ion currents, green  $^{13}\text{C}$  currents and red  $^{14}\text{C}$  normalized counts. The  $^{13}\text{C}/^{12}\text{C}$  ratio is indicated by yellow circles. Please note the flat region of the  $^{13}\text{C}/^{12}\text{C}$  isotope ratio in both scans ensuring long-term stable performance of the LEA system. Transparent green areas show possible magnetic field values for a stable measurement, while the blue lines indicate the values we chose for the measurements,  $B_{\text{LE}} = 428.0$  mT for the low energy magnet and  $B_{\text{HE}} = 847.2$  mT for the high energy magnet. Please note that since the isotopic beams are not perfectly Gaussian, the  $^{14}\text{C}$  peak in the HE-magnet scan is chosen slightly left to optimize the transmission. The rather narrow  $^{14}\text{C}$  scan is caused by another filter (electrostatic,  $E/q$  filter) that the  $^{14}\text{C}$  isotopes have to pass (see Figure 2).

detailed description of the adjustment technique can be found elsewhere (De Maria 2021). The LE and HE magnet scans are perfect tools to check the performance of the different isotope beams and to ensure stable long-term measurements. After the scans are taken, the magnetic fields are adjusted accordingly, as in our case  $B_{\text{LE}} = 428$  mT for the low energy magnet and  $B_{\text{HE}} = 847.2$  mT for the high energy magnet, indicated by blue lines in Figure 4. With these settings a transmission of 56% is achieved. The transmission is determined by the ratio of the  $^{12}\text{C}_{\text{HE}}^+$  beam current after the accelerator divided by the  $^{12}\text{C}_{\text{LE}}^-$  beam current before the accelerator or  $^{12}\text{C}_{\text{HE}}^+ / ^{12}\text{C}_{\text{LE}}^-$ . In comparison to the expected charge state yield of about 70% of the  $1^+$  charge state at 92 keV (Maxeiner et al. 2015b) this corresponds to  $\approx 80\%$  ion optical transmission of the LEA accelerator.

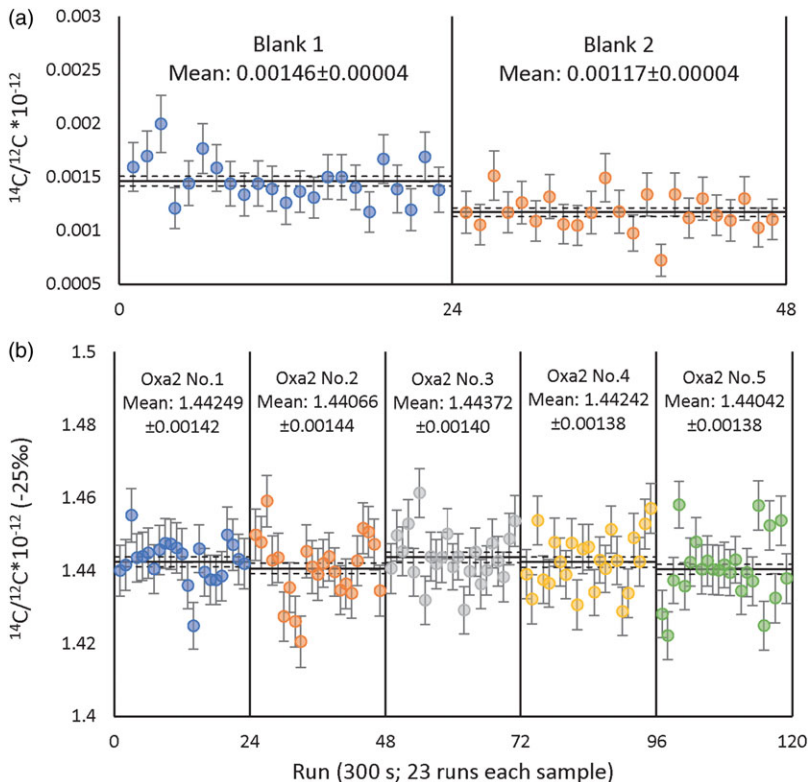


Figure 5 (a)  $^{14}\text{C}/^{12}\text{C}$  ratios measured for two phthalic acid blanks. Each run has a testing time of 300 s and 23 runs are taken of each sample. Statistical uncertainties are indicated by error bars, while mean values and their uncertainties are indicated by solid and dashed black lines, respectively. The radiocarbon age of blank 1 is more than 52,900 years ( $F^{14}\text{C} = 0.00138$ ) and blank 2 more than 54,600 years ( $F^{14}\text{C} = 0.00110$ ), which is not only a strong indication of a good measuring system, but also of clean sample preparation. (b)  $^{14}\text{C}/^{12}\text{C}$  ratios ( $^{13}\text{C}/^{12}\text{C}$  fractionation corrected) measured for five Oxalic Acid II standards. Each run has a testing time of 300 s and 23 runs are taken of each sample. The total number of  $^{14}\text{C}$  events detected is  $10^6$  counts per sample. Statistical uncertainties are indicated by error bars, while mean values and their uncertainties are indicated by solid and dashed black lines, respectively.

## Performance Tests

For the performance test a series of two PhA blanks as well as five Oxalic Acid II (Oxa2; SRM-4990C) standards (Mann 1983) are introduced to the LEA system, where each sample is analyzed in 23 runs of 300 s testing time. All samples are measured sequentially for a total of 23 runs. The measurements of two well prepared blanks are shown in Figure 5(a), blank 1 with a measured radiocarbon age of  $52,900 \text{ yr} \pm 250 \text{ yr}$  and blank 2 with  $54,700 \text{ yr} \pm 280 \text{ yr}$ , which are exceptionally good results in terms of both the quality of the measurements and the sample preparation. The blanks measured on LEA tend to be even older than measured on the MICADAS (Sookdeo et al. 2019), likely due to the implementation of an electrical field-free gap separating the conductance aperture at the exit of the stripper housing from the electric field section at the HE acceleration stage (see Figure 2).

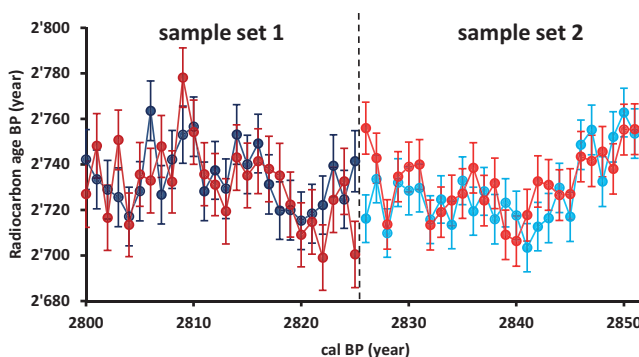


Figure 6 Dark blue (Data MICADAS set 1) and bright blue (Data MICADAS set 2) dots and lines in the diagram indicate data points of MICADAS measurements, while dark red (Data LEA set 1) and bright red (Data LEA set 2) dots and lines show data points of LEA measurements. The horizontal axis presents the (known) calendar age of the samples and the vertical axis illustrates the measured radiocarbon age. There is excellent agreement between the results of these measurements, showing a mean deviation of  $1.0 \pm 4.7$  yr ( $< 0.13 \pm 0.6\%$ ). In order to ensure sufficient counting statistics, a number of at least  $10^6$  detected  $^{14}\text{C}$  events is aimed for a standard sample (Oxa2).

The  $^{14}\text{C}/^{12}\text{C}$  ratio of five Oxa2 standards are given in Figure 5(b). The measured  $^{14}\text{C}/^{12}\text{C}$  ratios are normalized to a  $\delta^{13}\text{C}$  of  $-25\%$  according to (Stuiver and Polach 1977). While the raw data of  $^{14}\text{C}/^{12}\text{C}$  change by about 1% over the course of the measurement, there is no discernible trend in the fractionation-corrected  $^{14}\text{C}/^{12}\text{C}$  data. Notable here is the precision of the mean value of each sample, which is less than 1‰ for all samples. The mean of the means is  $(1.44191 \pm 0.00063) \times 10^{-12}$  (i.e., the statistical uncertainty of these measurements is less than 0.5‰). The standard deviation of 1.0‰ of the 5 measured standards is in good agreement with the uncertainty of the counting statistics of the individual measurements 0.9‰.

## LEA VS. MICADAS

As a final performance test, the LEA system is compared with the MICADAS system (Wacker et al. 2019). To carry out the tests two sets of samples, each composing of 7 standards, 4 blanks and 26 wood samples, are measured on both systems. The wood samples are consecutive annual rings of a tree of known age (age determined by dendrochronology). The experiments are taken as follows: First, one set of samples is measured on the LEA system shown in Figure 6 (cal BP 2800–2825, Data LEA 1). Then, these samples are taken out of the LEA system, transferred into the MICADAS system and measured equally (Data MICADAS 1), and vice versa for the second set of samples (cal BP 2826–2851, Data LEA 2 & MICADAS 2). In other words, the second set of samples is measured on MICADAS before it is measured on LEA. The agreement of the results is striking, as shown in Figure 6, with a mean deviation of these two AMS measurements of only  $1.0 \pm 4.7$  year. Please note that in these measurements, the first runs of each sample after insertion into the respective system are omitted as the sample materials have been exposed to air during the transfer of the magazines and therefore their surface may have become contaminated.

Table 1 Comparison of the specifications of the two AMS systems, MICADAS and LEA. The transmission ( $^{12}\text{C}_{\text{HE}}^+ / ^{12}\text{C}_{\text{LE}}^-$ ) is significantly higher with the LEA system but requires a lower beam current for stable measurements. Both properties determine the duration of the experiments, which is, overall, still shorter with the MICADAS system, providing the same level of precision. The accelerator is operated in a tandem configuration, resulting in the total energies for the isotopes being approximately 140 keV for LEA and 420 keV for MICADAS.

Specifications	MICADAS	LEA
Transmission	48%	56%
Blank	> 50,000 yr	> 50,000 yr
Oxa2 $^{14}\text{C}/^{12}\text{C}$ ratio	$1.54 \times 10^{-12}$	$1.50 \times 10^{-12}$
Oxa2 $^{13}\text{C}/^{12}\text{C}$ ratio	1.07%	1.09%
Precision Oxa2	1–2‰ @ >500k $^{14}\text{C}$	1–2‰ @ >500k $^{14}\text{C}$
Acceleration voltage	200 kV	50 kV
Source potential	40 kV	40 kV
$^{14}\text{C}$ detector	Ion chamber region	Proportional region
LE $^{12}\text{C}$ currents	40–60 $\mu\text{A}$ , max. 80 $\mu\text{A}$	25–40 $\mu\text{A}$ , max. 50 $\mu\text{A}$
Stripper gas	He, 1 <sup>+</sup> charge state	He, 1 <sup>+</sup> charge state

Table 1 compares the specifications of these two AMS systems. The approx. 20% higher transmission ratio of the LEA system is remarkable, representing an increase in efficiency, which in turn requires less sample material. However, the duration for the same experiment is presently still shorter for the MICADAS system, since MICADAS can be operated with roughly 50 % higher beam currents. To date, we have not seriously tested the LEA system with higher beam currents, but all previous experiments have shown that the best and most stable results are obtained with  $^{12}\text{C}$ -beam currents between 25 and 40  $\mu\text{A}$ .

## CONCLUSION

The LEA system is another step towards reaching the goal of a tabletop AMS system. With the reduction of the accelerator voltage to 50 kV, the overall dimensions of the system could be further reduced to  $2 \times 3 \text{ m}^2$ . A further reduction of the dimensions should be possible, such as through technical or constructional improvements or with a further reduction of the acceleration voltage.

The  $^{14}\text{C}$  background is excellent and exceeds results with most large AMS systems. Due to the compact design, the LEA system shows high measurement stability over time, though the optical transmission of the ion beam is reduced due to the relatively strong angular straggling of the low-energetic ion beam in the stripper. Consequently, highest precision measurements of 1–2‰ on modern samples are possible and compare well with measurements obtained with a larger, state-of-the-art MICADAS instrument.

## ACKNOWLEDGMENTS

We would like to thank K. Wyss, M. Alter, and K. Kündig for preparing the samples and J. Thut, R. Pfenninger, R. Gruber, P. Vogel, A. Wagner, T. Keller, and S. Bühlmann for technical support. We also thank the Swiss National Science Foundation for financially supporting this work (SNF grant number 200020\_197137).



## REFERENCES

- De Maria D. 2021. Towards a new horizon for biomedical applications of AMS, ETH Zurich, <https://doi.org/10.3929/ethz-b-000497563>
- Mann WB. 1983. An international reference material for radiocarbon dating. *Radiocarbon* 25(2):519–527.
- Maxeiner S, Seiler M, Suter M, Synal H-A. 2015a. Charge state distributions and charge exchange cross sections of carbon in helium at 30–258 keV. *Nuclear Instruments and Methods in Physics Research Section B: Beam Interactions with Materials and Atoms* 361:541–547.
- Maxeiner S, Suter M, Christl M, Synal H-A. 2015b. Simulation of ion beam scattering in a gas stripper. *Nuclear Instruments and Methods in Physics Research Section B: Beam Interactions with Materials and Atoms* 361:237–244.
- Maxeiner S, Synal H-A, Christl M, Suter M, Müller A, Vockenhuber C. 2019. Proof-of-principle of a compact 300 kV multi-isotope AMS facility. *Nuclear Instruments and Methods in Physics Research Section B: Beam Interactions with Materials and Atoms* 439:84–89.
- Müller AM, Döbeli M, Seiler M, Synal H-A. 2015. A simple Bragg detector design for AMS and IBA applications. *Nuclear Instruments and Methods in Physics Research Section B: Beam Interactions with Materials and Atoms* 356–357:81–87.
- Schulze-König T, Seiler M, Suter M, Wacker L, Synal HA. 2011. The dissociation of  $^{13}\text{CH}$  and  $^{12}\text{CH}_2$  molecules in He and  $\text{N}_2$  at beam energies of 80–250 keV and possible implications for radiocarbon mass spectrometry. *Nuclear Instruments and Methods in Physics Research Section B: Beam Interactions with Materials and Atoms* 269(1):34–39.
- Sookdeo A, Kromer B, Büntgen U, Friedrich M, Friedrich R, Helle G, Pauly M, Nievergelt D, Reinig F, Treydte K et al. 2019. Quality dating: a well-defined protocol implemented at ETH for high-precision  $^{14}\text{C}$ -dates tested on Late Glacial wood. *Radiocarbon* 62(4):891–899.
- Stuiver M, Polach HA. 1977. Discussion: reporting of  $^{14}\text{C}$  data. *Radiocarbon* 19(3):355–363.
- Sun G, Döbeli M, Müller AM, Stocker M, Suter M, Wacker L. 2007. Energy loss and straggling of heavy ions in silicon nitride in the low MeV energy range. *Nuclear Instruments and Methods in Physics Research Section B: Beam Interactions with Materials and Atoms* 256(2):586–590.
- Suter M, Döbeli M, Grajcar M, Müller A, Stocker M, Sun G, Synal H-A, Wacker L. 2007. Advances in particle identification in AMS at low energies. *Nuclear Instruments and Methods in Physics Research Section B: Beam Interactions with Materials and Atoms* 259(1):165–172.
- Suter M, Keith Fifield L, Maxeiner S. 2022. The impact of the break-up of molecules in the stripper on the AMS performance. *Nuclear Instruments and Methods in Physics Research Section B: Beam Interactions with Materials and Atoms* 533:96–103.
- Synal H-A, Stocker M, Suter M. 2007. MICADAS: a new compact radiocarbon AMS system. *Nuclear Instruments and Methods in Physics Research Section B: Beam Interactions with Materials and Atoms* 259(1):7–13.
- Wacker L, Bollhalder S, Sookdeo A, Synal HA. 2019. Re-evaluation of the New Oxalic Acid standard with AMS. *Nuclear Instruments and Methods in Physics Research Section B: Beam Interactions with Materials and Atoms* 455:178–180.